Author(s): Hinkkanen, M. & Leppanen, V.-M. & Luomi, J.

Title: Flux Observer Enhanced With Low-Frequency Signal Injection Allowing Sensorless Zero-Frequency Operation of Induction Motors

Year: 2005

Version: Post print

Please cite the original version:

Hinkkanen, M. & Leppanen, V.-M. & Luomi, J. 2005. Flux Observer Enhanced With Low-Frequency Signal Injection Allowing Sensorless Zero-Frequency Operation of Induction Motors. IEEE Transactions on Industry Applications. Volume 41, Issue 1. 52-59. ISSN 0093-9994 (printed). DOI: 10.1109/tia.2004.840958.

Flux Observer Enhanced with Low-Frequency Signal Injection Allowing Sensorless Zero-Frequency Operation of Induction Motors

Marko Hinkkanen, Veli-Matti Leppänen, and Jorma Luomi, *Member, IEEE*

***Abstract*—In sensorless induction motor drives, flux estimators based only on the standard motor model work well at sufficiently high stator frequencies, but they fail at frequencies close to zero. To solve this problem, a new observer structure is proposed, combining a speed-adaptive full-order flux observer with a low-frequency signal-injection method. An error signal obtained from the signal-injection method is used as an additional feedback signal in the speed-adaptation law of the observer, resulting in a wide speed range, excellent dynamic properties, and zero-frequency operation capability. The enhanced observer is also robust against parameter errors. Experimental results are shown, including very slow speed reversals and long-term zero-frequency operation under rated load torque, as well as rated load torque steps and fast speed reversals under rated load torque.**

***Index Terms*—Flux estimation, induction motor drives, signal injection, speed sensorless.**

I. Introduction

The research of the speed sensorless vector control of induction machines is motivated by the benefits in the cost of hardware and installation work and the reliability of the system. The estimation of the rotor flux is the crucial part of the control algorithm. It can be based on the standard motor model leading to, for example, the voltage model or the full-order flux observer. As the frequency approaches zero, however, the estimators based only on the standard motor model become increasingly sensitive to parameter errors. Even though operation at zero rotor speed at no load and under full load torque can be achieved [1], [2], more demanding operating points exist. Regenerating operation at very low stator frequencies has seldom been demonstrated (confusingly, the plugging mode is at low speeds often called the regenerating mode in the literature). Long-term operation at zero stator frequency under full load is not possible in practice.

For solving the problems encountered at low stator frequencies, various methods have been presented where a high-frequency test signal is superimposed on the stator voltage or current of the machine and information of the flux direction or rotor position is obtained from the response. Most of the signal-injection methods assume a spatial variation of the leakage inductance that is linked to the orientation of the flux [3], [4], or rotor position [5]. The rotor-position-dependent inductance variation can even be enhanced by design [6]–[8]. However, the signal carrying useful information is often corrupted by other signals of the same kind [9], [10], and additional machine-specific decoupling schemes must be devised [5], [8]. Some schemes employ the PWM switching waveform as an excitation [11], [12]. In [13], a resistance variation along the rotor periphery is introduced, and a periodic high-frequency voltage burst injection is used. Injecting a high-frequency voltage also causes a high-frequency zero-sequence voltage in a motor with main flux saturation. The amplitude variation of the high-frequency zero-sequence voltage can be used to track the air-gap flux [14]. A hybrid scheme combining a flux observer based on the standard motor model with a high-frequency signal-injection method is proposed in [15].

In a recently introduced controller [16], a low-frequency alternating current is superimposed on the flux-producing component of the stator current. The response of the mechanical system is used to adjust the test signal to coincide the direction of the rotor flux, provided that the total moment of inertia is not too high. The controller exhibits good steady-state performance down to zero-frequency operation, and it is insensitive to parameter errors. However, its dynamic response is only moderate.

In this paper, a speed-adaptive flux observer [17] based on the standard motor model is enhanced by the low-frequency signal-injection method [16] in order to obtain both fast response and stable zero-frequency operation despite of parameter errors. The speed-adaptation law is augmented with an error signal obtained from the signal-injection method. This additional correction also stabilizes the regenerating-mode low-speed operation. Simulations and experimental results demonstrate the system's stability and robustness against parameter errors.

II. Induction Motor Model

The standard dynamic model corresponding to the inverse-Γ-equivalent circuit [18] of the induction motor will be used. In a general reference frame, the voltage equations are

$$\underline{u}_s = R_s \underline{i}_s + \frac{d\underline{\psi}_s}{dt} + j\omega_k \underline{\psi}_s \tag{1a}$$

$$0 = R_R \underline{i}_R + \frac{d\underline{\psi}_R}{dt} + j\left(\omega_k - \omega_m\right)\underline{\psi}_R \tag{1b}$$

where $\underline{u}_s$ is the space vector of the stator voltage, $\underline{i}_s$ the space vector of the stator current, R_s the stator resistance, and ω_k the electrical angular speed of the reference frame. The rotor

M. Hinkkanen and J. Luomi are with the Power Electronics Laboratory, Helsinki University of Technology, FIN-02015 HUT, Espoo, Finland (email: marko.hinkkanen@hut.fi; jorma.luomi@hut.fi).

V.-M. Leppänen was with the Power Electronics Laboratory, Helsinki University of Technology, FIN-02015 HUT, Espoo, Finland. He is now with ABB Oy, FIN-00381 Helsinki, Finland (email: veli-matti.leppanen@fi.abb.com).

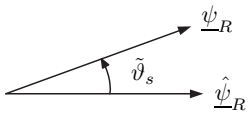

Fig. 1. Actual rotor flux $\underline{\psi}_R$ and estimated rotor flux $\hat{\underline{\psi}}_R$. The test signal alternates in the direction of the estimated rotor flux.

resistance is R_R, the rotor current $\underline{i}_R$, and the electrical angular speed of the rotor ω_m. The stator and rotor flux linkages are

$$\underline{\psi}_s = (L'_s + L_M)\,\underline{i}_s + L_M \underline{i}_R \tag{2a}$$

$$\underline{\psi}_R = L_M\,(\underline{i}_s + \underline{i}_R) \tag{2b}$$

respectively, where L_M and L'_s are the magnetizing inductance and the stator transient inductance, respectively.

The electromagnetic torque is given by

$$T_e = \frac{3}{2} p\,\mathrm{Im}\left\{\underline{i}_s \underline{\psi}_R^*\right\} \tag{3}$$

where the number of pole pairs is p and the complex conjugate is marked by the symbol *. The equation of motion is

$$\frac{d\omega_m}{dt} = \frac{p}{J}\,(T_e - T_L) \tag{4}$$

where the total moment of inertia of the mechanical system is J and the load torque is T_L. The back-emf used in this paper is defined by

$$\underline{e} = \left(\frac{1}{\tau_r} - j\omega_m\right) \underline{\psi}_R \tag{5}$$

where the rotor time constant is $\tau_r = L_M/R_R$.

The operating modes of the induction motor are defined here using the relative slip ω_r/ω_s, where the angular speed of the rotor flux is ω_s and the angular slip frequency $\omega_r = \omega_s - \omega_m$. The operating modes are [19]:

1) regenerating mode ($\omega_r/\omega_s < 0$);
2) motoring mode ($0 < \omega_r/\omega_s < 1$);
3) plugging mode ($\omega_r/\omega_s > 1$).

To recognize the plugging mode more easily, the condition for it can also be expressed as $\omega_m \omega_s < 0$. Operation in the regenerating mode at low stator frequencies is generally the most demanding working point of sensorless induction motor drives. Operation at zero stator frequency under load torque can be interpreted as a borderline case of the regenerating mode.

III. Signal Injection and Its Response

In the following, the angle of the rotor flux is ϑ_s and the angle of the estimated rotor flux $\hat{\vartheta}_s$. The error angle is $\tilde{\vartheta}_s = \vartheta_s - \hat{\vartheta}_s$ as illustrated in Fig. 1. Since $\tilde{\vartheta}_s$ is not explicitly known, an error signal F_ϑ having the same sign as $\tilde{\vartheta}_s$ will be introduced.

A. Back-EMF Response in Rotor Flux Reference Frame

As shown in Fig. 2, an ac test signal $A\cos(\omega_c t)$ is superimposed on the d-component of the stator current in the estimated rotor flux reference frame, the d-axis of which is at angle $\hat{\vartheta}_s$ relative to the stationary reference frame [16].

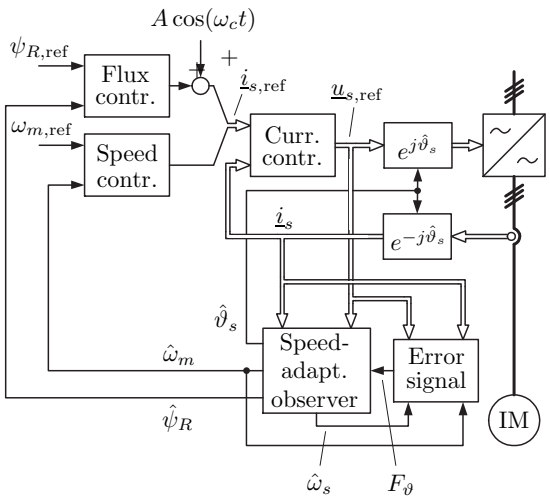

Fig. 2. Rotor flux oriented controller using flux observer enhanced with low-frequency signal injection. An ac test signal is superimposed on the d-component of the stator current. The block "Error signal" is shown in Fig. 3.

Thus the spatial angle of the ac test signal is $-\tilde{\vartheta}_s$ in the rotor flux reference frame, where the test signal appears as a vector $(\cos\tilde{\vartheta}_s - j\sin\tilde{\vartheta}_s)A\cos(\omega_c t)$.

If $\tilde{\vartheta}_s = 0$, the test signal causes predominantly an alternating component in the flux amplitude. This oscillation and its effects are small, and they can be compensated [20]. Furthermore, the saturation of the magnetizing inductance decreases the oscillation in the flux magnitude. If $\tilde{\vartheta}_s \neq 0$, the test signal has a true q-component which, according to (3), creates a torque oscillation

$$T_{ec}(t) = -\frac{3}{2} p \psi_{R0} A\cos(\omega_c t)\sin\tilde{\vartheta}_s \tag{6}$$

where ψ_{R0} is the amplitude of the rotor flux at the quiescent operating point. Based on (4), the oscillating torque causes an oscillation in the rotor speed, and further an oscillation

$$e^k_{qc}(t) = \frac{3p^2\psi^2_{R0}}{2J\omega_c} A\sin(\omega_c t)\sin\tilde{\vartheta}_s \tag{7}$$

in the q-component of the back-emf (the superscript k indicates the rotor flux reference frame).

B. Error Signal in Estimated Rotor Flux Reference Frame

The analysis above suggests that multiplying the back-emf response $e^k_{qc}(t)$ by $\sin(\omega_c t)$ will give a signal having the same sign as $\tilde{\vartheta}_s$. Since ϑ_s is not known in practice, the actual component $e^k_{qc}(t)$ is not accessible. Instead, the corresponding q-component in the estimated rotor flux reference frame (where the test signal appears real) is used. The response in the estimated rotor flux reference frame is approximately [20]

$$e_{qc}(t) = \left[\left(\frac{3p^2\psi^2_{R0}}{2J} + \frac{R_R}{\tau_r}\right)\tilde{\vartheta}_s - \omega_{m0} R_R\right]\frac{A}{\omega_c}\sin(\omega_c t) \tag{8}$$

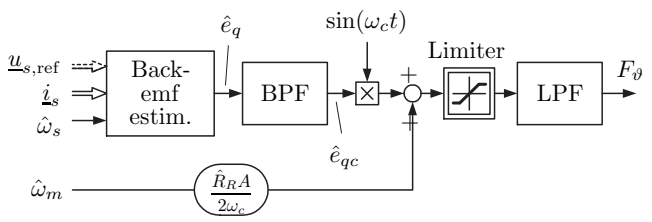

Fig. 3. Calculation of the error signal F_ϑ in the estimated rotor flux reference frame.

where ω_{m0} is the rotor speed at the quiescent operating point. In practice, the response is estimated from the stator voltage and current using a band-pass-filter (BPF),

$$\hat{e}_{qc}(t) = \mathrm{BPF}\Big\{-u_{sq,\mathrm{ref}} + \hat{L}'_s \frac{di_{sq}}{dt} + \hat{\omega}_s \hat{L}'_s i_{sd} + (\hat{R}_s + \hat{R}_R) i_{sq}\Big\} \tag{9}$$

where $\hat{\omega}_s$ is the angular speed of the rotor flux estimate and parameter estimates are marked by the symbol $\hat{}$. The q-component of the reference voltage $u_{sq,\mathrm{ref}}$ and the stator current components i_{sd} and i_{sq} are in the estimated rotor flux reference frame.

The estimate of the part independent of $\tilde{\vartheta}_s$ in (8) is subtracted from $\hat{e}_{qc}(t)$ and the result is demodulated. Multiplication by $\sin(\omega_c t)$ gives the function

$$f_\vartheta(t) = \left[\hat{e}_{qc}(t) + \hat{\omega}_{m0}\hat{R}_R \frac{A}{\omega_c}\sin(\omega_c t)\right]\sin(\omega_c t) \tag{10}$$

where $\hat{\omega}_{m0}$ is the estimated rotor speed at the quiescent operating point. Low-pass filtering (LPF) of f_ϑ gives an error signal voltage

$$\begin{aligned} F_\vartheta &= \mathrm{LPF}\big\{f_\vartheta\big\} \\ &\approx \left[\left(\frac{3p^2\psi_{R0}^2}{2J} + \frac{R_R}{\tau_r}\right)\tilde{\vartheta}_s - \omega_{m0}R_R + \hat{\omega}_{m0}\hat{R}_R\right]\frac{A}{2\omega_c} \end{aligned} \tag{11}$$

which is constant in steady state. Fig. 3 shows the block diagram of the error signal calculation, which will be explained in more detail in Section V.

Generally, a larger gain $F_\vartheta/\tilde{\vartheta}_s$ results in a better signal-to-noise ratio. According to (11), the gain $F_\vartheta/\tilde{\vartheta}_s$ can be increased by increasing the amplitude A or decreasing the frequency ω_c. However, decreasing ω_c decreases the achievable dynamics of F_ϑ.

IV. Speed-Adaptive Flux Observer

The full-order flux observer using the state vector $\hat{\underline{\mathbf{x}}} = [\hat{\underline{\psi}}_s \quad \hat{\underline{\psi}}_R]^T$ is defined by

$$\frac{d\hat{\underline{\mathbf{x}}}}{dt} = \hat{\underline{\mathbf{A}}}\,\hat{\underline{\mathbf{x}}} + \mathbf{B}\underline{u}_s + \underline{\mathbf{L}}\big(\underline{i}_s - \hat{\underline{i}}_s\big) \tag{12a}$$

$$\hat{\underline{i}}_s = \hat{\mathbf{C}}\hat{\underline{\mathbf{x}}} \tag{12b}$$

The system matrices are $\mathbf{B} = [1 \quad 0]^T$, $\hat{\mathbf{C}} = [1/\hat{L}'_s \quad -1/\hat{L}'_s]$, and

$$\hat{\underline{\mathbf{A}}} = \begin{bmatrix} -\frac{1}{\hat{\tau}'_s} - j\omega_k & \frac{1}{\hat{\tau}'_s} \\ \frac{1-\hat{\sigma}}{\hat{\tau}'_r} & -\frac{1}{\hat{\tau}'_r} - j(\omega_k - \hat{\omega}_m) \end{bmatrix} \tag{12c}$$

where the parameter estimates are $\hat{\sigma} = \hat{L}'_s/(\hat{L}_M + \hat{L}'_s)$, $\hat{\tau}'_s = \hat{L}'_s/\hat{R}_s$, and $\hat{\tau}'_r = \hat{\sigma}\hat{L}_M/\hat{R}_R$. The observer gain

$$\underline{\mathbf{L}} = \begin{bmatrix} \underline{l}_s \\ \underline{l}_r \end{bmatrix} = \lambda \begin{bmatrix} 1 + j\,\mathrm{sign}(\hat{\omega}_m) \\ -1 + j\,\mathrm{sign}(\hat{\omega}_m) \end{bmatrix} \tag{13a}$$

where

$$\lambda = \begin{cases} \lambda' \frac{|\hat{\omega}_m|}{\omega_\lambda}, & \text{if } |\hat{\omega}_m| < \omega_\lambda \\ \lambda', & \text{if } |\hat{\omega}_m| \geq \omega_\lambda \end{cases} \tag{13b}$$

gives satisfactory behavior from zero speed to very high speeds [17]. Parameters λ' and ω_λ are positive constants.

A. Speed Adaptation Without Signal Injection

Conventionally, the rotor speed is estimated using the adaptation law

$$\hat{\omega}_m = -\gamma_p \varepsilon - \gamma_i \int \varepsilon dt \tag{14}$$

where γ_p and γ_i are positive adaptation gains and

$$\varepsilon = \mathrm{Im}\left\{\big(\underline{i}_s - \hat{\underline{i}}_s\big)\hat{\underline{\psi}}_R^*\right\} \tag{15}$$

is an error term. With accurate motor parameter estimates, the adaptation law using (15) works well except at low speeds in the regenerating mode.

The regenerating mode can be stabilized, for example, by using a modified error term [2]. However, an inaccurate stator resistance estimate causes problems at low stator frequencies. This well-known problem is also encountered with other flux estimators based on the standard motor model. Especially, long-term operation under full load torque close to zero stator frequency is difficult. Fortunately, the accuracy of the stator resistance estimate is not that crucial during transients.

B. Speed Adaptation Enhanced With Signal Injection

If the error angle $\tilde{\vartheta}_s$ were known, the error term $\varepsilon = \tilde{\vartheta}_s$ would result in a robust system having good dynamics. In practice, the signal F_ϑ approximately proportional to $\tilde{\vartheta}_s$ is available. However, F_ϑ has a limited bandwidth due to the delays and filtering needed in the demodulation process.

The steady-state robustness of the low-frequency signal-injection method and the fast response of the speed-adaptive flux observer can be combined by using the error term

$$\varepsilon = \mathrm{Im}\left\{\big(\underline{i}_s - \hat{\underline{i}}_s\big)\hat{\underline{\psi}}_R^*\right\} + \gamma_\vartheta F_\vartheta \tag{16}$$

where γ_ϑ is a positive gain. The error term (16) makes long-term zero-frequency operation possible without losing the dynamic performance. Furthermore, the correction provided by the signal-injection method stabilizes the regenerating mode at low speeds, even with an inaccurate stator resistance estimate. It is to be noted that the signal F_ϑ is not generally driven to zero with (16).

The robustness can be increased further by driving the signal F_ϑ to zero by using the error term

$$\varepsilon = \mathrm{HPF}\left\{\mathrm{Im}\big\{\big(\underline{i}_s - \hat{\underline{i}}_s\big)\hat{\underline{\psi}}_R^*\big\}\right\} + \gamma_\vartheta F_\vartheta \tag{17}$$

where a first-order high-pass filter (HPF) $s/(s+\alpha_i)$ having the corner frequency α_i is used. In [15], the high-frequency

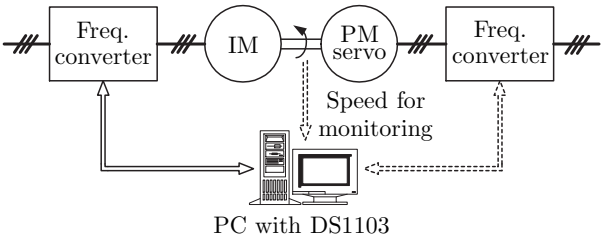

Fig. 4. Experimental setup. Permanent magnet (PM) servo motor was used as loading machine.

signal-injection method was combined with a speed-adaptive flux observer in a fashion similar to (17).

The high-pass filter in (17) may slightly deteriorate the transient performance. This can be circumvented by using the low-pass-filter-based realization of the high-pass filter

$$\frac{s}{s+\alpha_i} = 1 - \underbrace{\frac{\alpha_i}{s+\alpha_i}}_{\text{low-pass path}} \tag{18}$$

where the state of the low-pass path is reset and limited suitably. Resetting is carried out in the beginning of transients, which can be detected, for example, by monitoring the error $\omega_{m,\mathrm{ref}} - \hat{\omega}_m$ (where $\omega_{m,\mathrm{ref}}$ is the speed reference).

Weak fluctuations in the estimated variables may appear at standstill at no load when the error term (17) is used. These low-frequency fluctuations can be suppressed by rotating the current estimation error by factor $\exp(-j\phi)$ as

$$\varepsilon = \mathrm{HPF}\left\{\mathrm{Im}\{(\underline{i}_s - \underline{\hat{i}}_s)\underline{\hat{\psi}}_R^* e^{-j\phi}\}\right\} + \gamma_\vartheta F_\vartheta \tag{19}$$

where the angle ϕ is nonzero only in the regenerating mode at very low loads and speeds. A similar modification of the error term have been used for stabilizing the regenerating mode without signal injection [2].

V. Control System

The operation of the enhanced observer using the speed-adaptation law (19) was investigated by means of simulations and experiments. The MATLAB/Simulink environment was used for the simulations. The experimental setup is shown in Fig. 4. A 2.2-kW four-pole induction motor (IM) is fed by a frequency converter controlled by a dSpace DS1103 PPC/DSP board. The parameters of the induction motor are given in Table I. The total moment of inertia of the experimental setup is 2.2 times the inertia of the induction motor rotor. The control system used in the simulations and experiments is based on rotor flux orientation. The simplified overall block diagram of the system is shown in Fig. 2.

A. Controllers and Flux Observer

A PI-type synchronous-frame current controller is used [21]. The bandwidth of the current controller is 8 p.u., where the base value of the angular frequency is $2\pi \cdot 50$ rad/s. The speed estimate for the speed controller is filtered using a first-order low-pass filter having the bandwidth of 0.8 p.u., and the speed controller is a conventional PI-controller having the bandwidth of 0.16 p.u. The flux controller is a PI-type controller having the bandwidth of 0.016 p.u. in the base-speed region. The flux reference in the base-speed region is $\psi_{R,\mathrm{ref}} = 0.9$ Wb.

TABLE I
Parameters of the 2.2-kW Four-Pole 400-V 50-Hz Motor

Stator resistance R_s	3.67 Ω
Rotor resistance R_R	2.10 Ω
Stator transient inductance L'_s	0.0209 H
Magnetizing inductance L_M	0.224 H
Total moment of inertia J	0.0155 kgm^2
Rated speed	1 430 r/min
Rated current	5.0 A
Rated torque	14.6 Nm

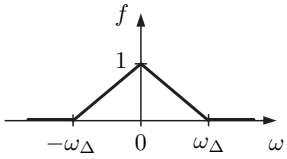

Fig. 5. Function $f(\omega)$. Different values for ω_Δ are used in (20) and (21).

For the speed-adaptive flux observer, the parameters $\lambda' = 10\ \Omega$ and $\omega_\lambda = 1$ p.u. are used in (13). The speed-adaptation gains in (14) are $\gamma_p = 10$ rad/(s·Nm) and $\gamma_i = 10\,000$ rad/(s^2·Nm). The digital implementation in the estimated rotor flux reference frame is used [22].

The sampling is synchronized to the modulation, and both the switching frequency and the sampling frequency are 5 kHz. The dc-link voltage is measured, and the reference voltage obtained from the current controller is used for the flux observer. A simple current feedforward compensation for dead times and power device voltage drops is applied [23].

B. Signal Injection

The frequency of the test signal is 25 Hz (i.e., $\omega_c = 0.5$ p.u.), which gives, according to (11), $F_\vartheta/\tilde{\vartheta}_s \approx 1.06$ V/rad in the experimental setup. In order to obtain a smooth transition between the low-speed signal-injection region and normal operating region, the signal-injection parameters are varied according to

$$A = f(\hat{\omega}_s)A_0, \quad \gamma_\vartheta = f(\hat{\omega}_s)\gamma_{\vartheta 0}, \quad \alpha_i = f(\hat{\omega}_s)\alpha_{i0} \tag{20}$$

where $\hat{\omega}_s$ is the angular speed of the rotor flux estimate. The function f is shown graphically in Fig. 5. The values corresponding to zero-frequency operation are $A_0 = 1$ A, $\gamma_{\vartheta 0} = 2$ Nm/V, and $\alpha_{i0} = 0.016$ p.u., and the transition speed is $\omega_\Delta = 0.16$ p.u.

The angle ϕ in (19) is selected according to

$$\phi = \begin{cases} \phi_{\max}\,\mathrm{sign}(\hat{\omega}_s) f(\hat{\omega}_m) f(\hat{\omega}_r), & \text{if } \hat{\omega}_s\hat{\omega}_r < 0 \\ 0, & \text{otherwise} \end{cases} \tag{21}$$

where $\hat{\omega}_r = \hat{\omega}_s - \hat{\omega}_m$ is the angular slip frequency estimate, and the function f shown in Fig. 5 is used. The angle $\phi_{\max} = 0.15\pi$ rad and $\omega_\Delta = 0.005$ p.u. are used in (21).

The low-pass path of (18) is limited to 0.2 Wb $\cdot |i_{sq}| f(\hat{\omega}_s)$, where i_{sq} is the q component of the stator current in the

estimated rotor flux reference frame. Furthermore, the low-pass path is reset when $|\omega_{m,\mathrm{ref}} - \hat{\omega}_m| > 0.03$ p.u.

The error signal F_ϑ is calculated according to Fig. 3. Instead of using a band-pass filter, the filtering of $\hat{e}_q$ is achieved by zero averaging and removing the trend over one period of the injection signal [16],

$$\hat{e}_{qc}(t) = \hat{e}_q(t) - \frac{1}{T_c}\int_{t-T_c}^{t} \hat{e}_q(t)dt - \frac{1}{2}\frac{d}{dt}\int_{t-T_c}^{t} \hat{e}_q(t)dt \quad (22)$$

where $T_c = 2\pi/\omega_c$. The first-order low-pass filter in Fig. 3 has the bandwidth of 0.16 p.u. Prior to filtering, the amplitude of F_ϑ is limited to ± 0.3 V.

VI. Results

Constant-valued estimates of the motor parameters are used in all simulations and experiments. The base values used in the following figures are: current $\sqrt{2}$·5.0 A, flux 1.04 Wb, and angular frequency 2π·50 rad/s.

A. Simulations

Robustness against errors in parameter estimates is studied by means of simulations. In the motor model of the simulator, the measured magnetizing inductance depicted in Fig. 6 is used, whereas other motor parameters are constant.

An example of simulation results showing slow speed reversals is shown in Fig. 7, where an inaccurate stator resistance estimate $\hat{R}_s = 1.2R_s$ is used. A rated load torque step was applied at $t = 5$ s. The speed reference was changed linearly from 0.06 p.u. to -0.06 p.u. when $t = 10\ldots80$ s, and then back to 0.06 p.u. when $t = 80\ldots150$ s. The drive operates first in the motoring mode, then in the plugging mode ($t \approx 45\ldots63$ s), in the regenerating mode ($t \approx 63\ldots97$ s), again in the plugging mode ($t \approx 97\ldots115$ s), and finally again in the motoring mode. It can be seen that the system is stable in all three operating modes of the induction motor.

Simulations corresponding to Fig. 7 using inaccurate $\hat{L}'_s$, $\hat{R}_R$, and $\hat{L}_M$ were also carried out (one erroneous estimate at a time, errors larger than 50 % not tested). The range for stable operation for the parameter estimates is given in Table II. As assumed, the only critical parameter is the stator resistance estimate $\hat{R}_s$. The maximum error in $\hat{R}_s$ is determined by the load torque step at $t = 5$ s while a larger error is allowed in the other parts of the sequence.

The same system using estimators based only on the standard motor model, e.g., [2], [24], can cope with the sequence of Fig. 7 if the error in $\hat{R}_s$ is less than approximately one percent. Furthermore, many estimators, e.g., [25], [26], are unstable in the regenerating mode when $t \approx 63\ldots97$ s even if all parameter estimates are accurate.

B. Experiments

Experimental results of slow speed reversals are shown in Fig. 8, where the test sequence is equal to that in Fig. 7. The system is stable in all three operating modes of the induction motor. This kind of very slow speed reversal is not possible without the signal-injection based correction. On the other hand, the low-frequency signal-injection method without the speed-adaptive flux observer would not tolerate the rated load torque step at $t = 5$ s.

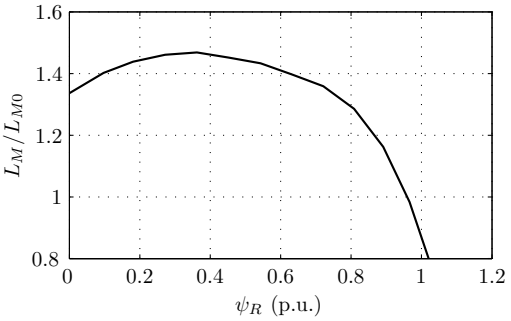

Fig. 6. Measured magnetizing inductance of the 2.2-kW motor. Base value of the flux is 1.04 Wb and $L_{M0} = 0.224$ H.

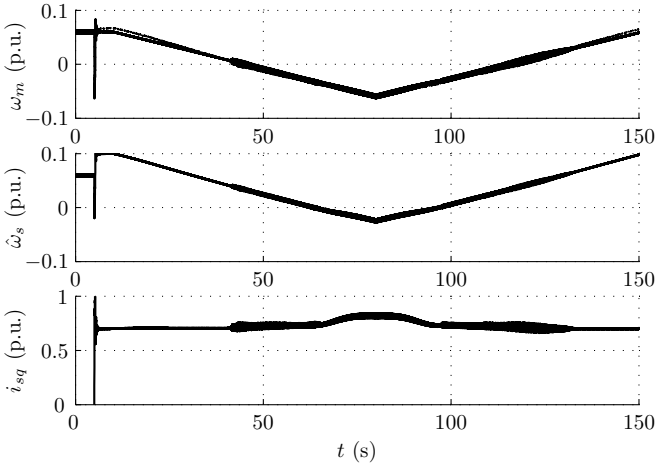

Fig. 7. Simulation results: slow speed reversals under rated load torque, $\hat{R}_s = 1.2R_s$. The first subplot shows the measured speed (solid) and the estimated speed (dotted). The second subplot shows the angular frequency of the estimated rotor flux. The third subplot presents the q component of the stator current in the estimated rotor flux reference frame.

Experimental results showing zero-speed operation and a rated load torque step are shown in Fig. 9. The flux components in the stator reference frame are marked by the subscripts α and β. The speed reference was set to zero. A rated load torque step was applied at $t = 2$ s, and the load torque was removed at $t = 10$ s. It can be seen that both the flux and the speed are correctly observed. After removing the load, the flux is still properly estimated and the load torque could be applied again. For this kind of sequence, the correction by the signal injection would not be necessary.

Fig. 10 depicts experimental results of operation at zero stator frequency. The speed reference was set to 0.033 p.u., and a negative rated load torque step was applied at $t = 5$ s. After applying the negative load, the drive operates at zero stator frequency as can be seen from the components of the estimated flux. The load torque was removed at $t = 55$ s. It can be seen that stable zero-frequency operation under load torque is achieved. The speed-adaptive flux observer [17] without the signal injection would collapse soon after the load torque step (at $t \approx 6$ s), whereas the low-frequency signal-injection

TABLE II
RANGE FOR STABLE OPERATION IN SIMULATION SEQUENCE OF FIG. 7

Parameter estimate	Range for stable operation
$\hat{R}_s$	$0.87R_s \ldots 1.2R_s$
$\hat{R}_R$	$0.5R_R \ldots 1.5R_R$
$\hat{L}'_s$	$0.5L'_s \ldots 1.5L'_s$
$\hat{L}_M$	$0.5L_M \ldots 1.25L_M$

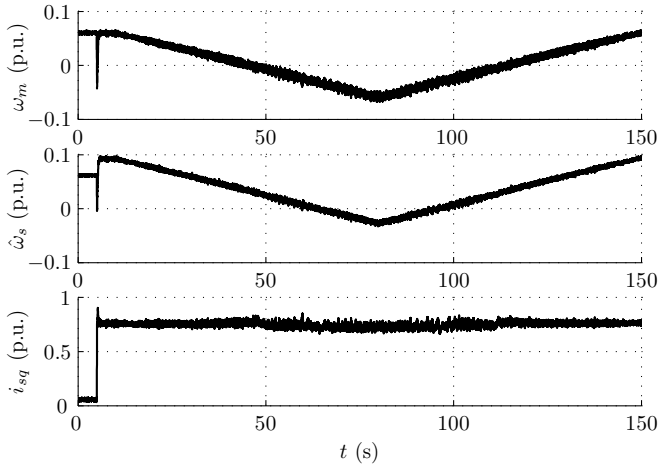

Fig. 8. Experimental results: slow speed reversals under rated load torque. Explanations of curves as in Fig. 7.

method alone could not handle the load torque steps.

Zero-speed operation during a slow load torque reversal is depicted in Fig. 11. The speed reference was set to zero, and the load torque was decreased linearly from the positive rated value to the negative rated value in 60 seconds. Due to the signal injection, no problems were encountered. For observers without signal injection, this kind of load torque reversals are usually more difficult than load torque steps at zero speed. The reason is the stator frequency remaining in the vicinity of zero for a long time.

A stepwise reversal of the load torque is shown in Fig. 12. The speed reference was set to 0.02 p.u. A positive rated load torque step was applied at $t = 2$ s, and the load torque was reversed at $t = 8$ s. The system is stable both in the motoring mode ($t = 0 \ldots 8$ s) and in the plugging mode ($t = 8 \ldots 15$ s), and during the step change in the load torque. The observer without the signal injection would be stable in this sequence, but $\hat{R}_s$ should be more accurate than with the signal-injection correction.

Fig. 13 shows a stepwise speed reference change under rated load torque. The speed reference was initially set to 0.02 p.u., and the load torque step was applied at $t = 2$ s. The speed reference was stepped to -0.04 p.u. at $t = 6$ s while the load torque was still applied. The system is stable in the motoring mode ($t = 0 \ldots 6$ s), during the step change in the speed reference, and in the regenerating mode ($t = 6 \ldots 20$ s). The observer without the signal injection could not operate continuously in the regenerating mode due to low stator frequency (approximately 0.008 p.u.). For observers based only on the standard motor model, this sequence is generally

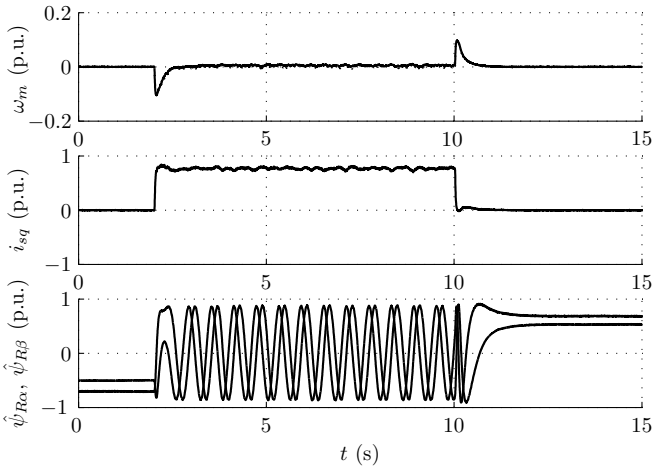

Fig. 9. Experimental results: zero-speed operation when rated load torque step applied. The first subplot shows the measured speed (solid) and the estimated speed (dotted). The second subplot shows the q component of the stator current in the estimated rotor flux reference frame. The third subplot presents the real and imaginary components of the estimated rotor flux in the stator reference frame.

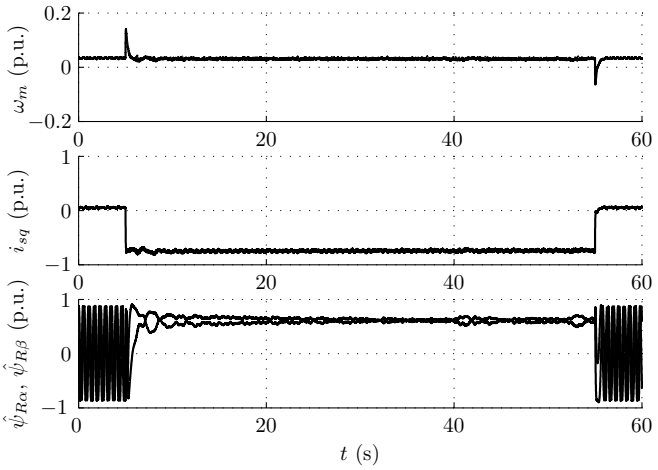

Fig. 10. Experimental results: operation at zero stator frequency under rated load torque. Explanations of curves as in Fig. 9.

more difficult than the sequences in Figs. 9 and 12 (even though the absolute value of the rotor speed is higher). The low-frequency noise appearing in the regenerating mode may originate from the incomplete dead-time compensation; it was not seen in the corresponding simulations. The effect of the dead-time compensation is more significant in the regenerating mode than in the motoring mode since the amplitude of the stator voltage is smaller.

Fast transitions between the signal-injection region and the normal operating region are shown in Fig. 14. The speed reference was initially zero, and it was changed to -0.6 p.u. at $t = 1$ s and to 0.6 p.u. at $t = 2$ s. The rated load torque step was applied at $t = 3$ s. The speed reference was set to zero at $t = 4$ s while the rated load torque was still applied. It can be seen that no problems are encountered during the transitions. The observer without the signal injection would cope with this sequence, assuming a small error in $\hat{R}_s$. The response of the low-frequency signal-injection method alone would be slower,

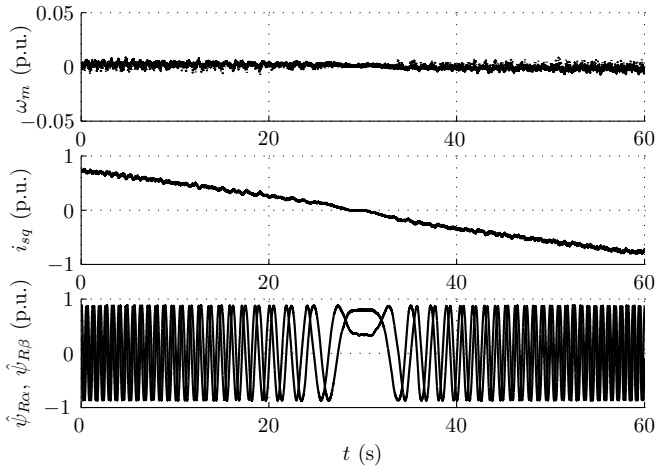

Fig. 11. Experimental results: slow load torque reversal at zero speed reference. Explanations of curves as in Fig. 9.

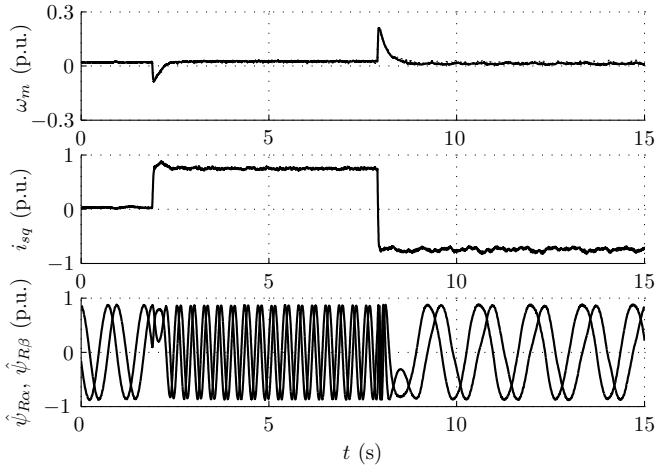

Fig. 12. Experimental results: stepwise load torque reversal. Explanations of curves as in Fig. 9.

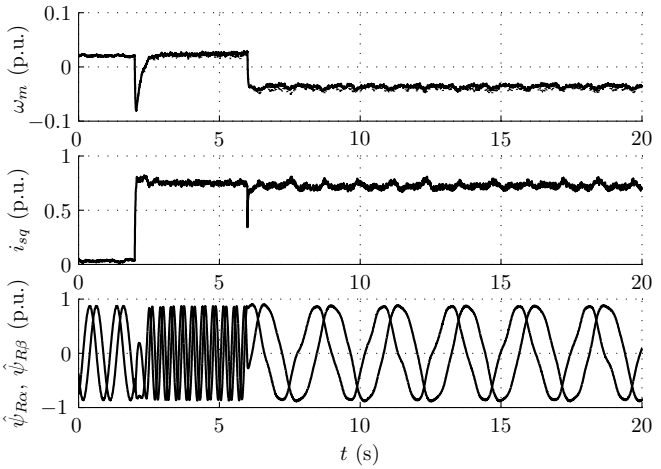

Fig. 13. Experimental results: stepwise speed reference change under rated load torque. Explanations of curves as in Fig. 9.

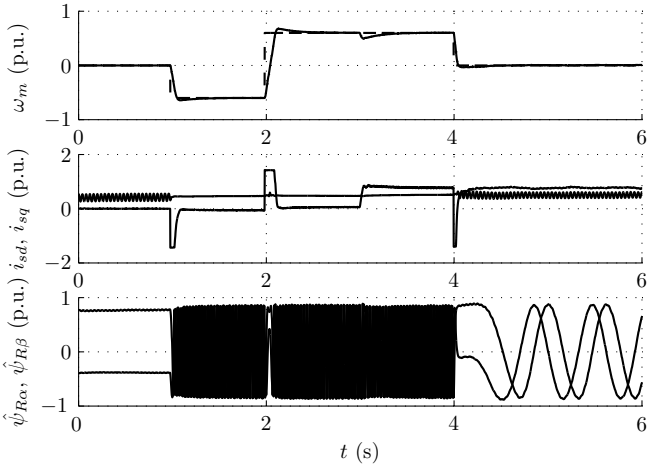

Fig. 14. Experimental results: fast transitions between signal-injection region and normal operating region. Explanations of curves as in Fig. 9. Speed reference (dashed line in the first subplot) and the d component of the stator current (in the second subplot) are also presented.

and it would not tolerate the rated load torque step.

VII. Conclusions

A new observer structure was proposed, combining a speed-adaptive full-order flux observer with a low-frequency signal-injection method. A low-frequency ac test signal is superimposed on the stator current. The response in the stator voltage depends on the orientation of the signal relative to that of the rotor flux. The dependency is due to the reaction of the mechanical system, and it can be used to enhance the low-speed operation of the speed-adaptive flux observer. An error signal obtained from the signal-injection method is used as an additional correction in the speed-adaptation law.

Experimental results have shown that the combination yields an observer exhibiting both fast response and steady-state robustness against parameter errors down to zero stator frequency. Stable operation in all three operating modes (motoring, regenerating, and plugging) of the induction motor have been demonstrated.

A suitable topic for future research is to investigate whether an on-line stator resistance estimator can be incorporated into the proposed observer without impairing stability. It might also be possible to use the low-frequency signal-injection method to estimate the stator resistance.

Acknowledgment

The authors gratefully acknowledge the financial support given by ABB Oy and the Finnish Cultural Foundation.

References

[1] J. Holtz and J. Quan, "Drift- and parameter-compensated flux estimator for persistent zero-stator-frequency operation of sensorless-controlled induction motors," *IEEE Trans. Ind. Applicat.*, vol. 39, no. 4, pp. 1052–1060, July/Aug. 2003.

[2] M. Hinkkanen and J. Luomi, "Stabilization of regenerating mode operation in sensorless induction motor drives by full-order flux observer design," *IEEE Trans. Ind. Electron.*, vol. 51, no. 6, pp. 1318–1328, Dec. 2004.

[3] P. L. Jansen and R. D. Lorenz, "Transducerless field orientation concepts employing saturation-induced saliences in induction machines," *IEEE Trans. Ind. Applicat.*, vol. 32, no. 6, pp. 1380–1393, Nov./Dec. 1996.

[4] J.-I. Ha, S.-K. Sul, K. Ide, I. Murokita, and K. Sawamura, "Physical understanding of high frequency injection method to sensorless drives of an induction machine," in *Conf. Rec. IEEE-IAS Annu. Meeting*, vol. 3, Rome, Italy, Oct. 2000, pp. 1802–1808.

[5] N. Teske, G. M. Asher, M. Sumner, and K. J. Bradley, "Encoderless position estimation for symmetric cage induction motor under loaded conditions," *IEEE Trans. Ind. Applicat.*, vol. 37, no. 6, pp. 1793–1800, Nov./Dec. 2001.

[6] P. L. Jansen and R. D. Lorenz, "Transducerless position and velocity estimation in induction and salient AC machines," *IEEE Trans. Ind. Applicat.*, vol. 31, no. 2, pp. 240–247, Mar./Apr. 1995.

[7] J. Cilia, G. M. Asher, K. J. Bradley, and M. Sumner, "Sensorless position detection for vector-controlled induction motor drives using an asymmetric outer-section cage," *IEEE Trans. Ind. Applicat.*, vol. 33, no. 5, pp. 1162–1169, Sept./Oct. 1997.

[8] F. Briz, M. W. Degner, A. Diez, and R. D. Lorenz, "Measuring, modeling, and decoupling of saturation-induced saliencies in carrier-signal injection-based sensorless AC drives," *IEEE Trans. Ind. Applicat.*, vol. 37, no. 5, pp. 1356–1364, Sept./Oct. 2001.

[9] M. L. Aime, M. W. Degner, and R. D. Lorenz, "Saturation measurements in AC machines using carrier signal injection," in *Conf. Rec. IEEE-IAS Annu. Meeting*, vol. 1, St. Louis, MO, Oct. 1998, pp. 159–166.

[10] T. Wolbank and B. Haidvogl, "Evaluation of the influence of design and operation of standard induction motors on sensorless control schemes utilizing saliencies in the transient electrical behaviour," in *Proc. IEEE PESC'00*, vol. 2, Galway, Ireland, June 2000, pp. 903–908.

[11] M. Schroedl, "Sensorless control of AC machines at low speed and standstill based on the "INFORM" method," in *Conf. Rec. IEEE-IAS Annu. Meeting*, vol. 2, San Diego, CA, Oct. 1996, pp. 270–277.

[12] J. Holtz, J. Jiang, and H. Pan, "Identification of rotor position and speed of standard induction motors at low speed including zero stator frequency," in *Proc. IEEE IECON'97*, vol. 2, New Orleans, LA, Nov. 1997, pp. 971–976.

[13] C. S. Staines, G. M. Asher, and K. J. Bradley, "A periodic burst injection method for deriving rotor position in saturated cage-salient induction motors without a shaft encoder," *IEEE Trans. Ind. Applicat.*, vol. 35, no. 4, pp. 851–858, July/Aug. 1999.

[14] A. Consoli, G. Scarcella, A. Testa, and T. A. Lipo, "Air-gap flux position estimation of inaccessible neutral induction machines by zero-sequence voltage," *Electr. Power Comp. Syst.*, vol. 30, no. 1, pp. 77–88, Jan. 2002.

[15] K. Ide, J.-I. Ha, M. Sawamura, H. Iura, and Y. Yamamoto, "A novel hybrid speed estimator of flux observer for induction motor drives," in *Proc. IEEE ISIE'02*, vol. 3, L'Aquila, Italy, July 2002, pp. 822–827.

[16] V.-M. Leppänen and J. Luomi, "Rotor flux angle tracking controller for sensorless induction motor drives," in *Conf. Rec. IEEE-IAS Annu. Meeting*, vol. 2, Pittsburgh, PA, Oct. 2002, pp. 856–863.

[17] M. Hinkkanen, "Analysis and design of full-order flux observers for sensorless induction motors," *IEEE Trans. Ind. Electron.*, vol. 51, no. 5, pp. 1033–1040, Oct. 2004.

[18] G. R. Slemon, "Modelling of induction machines for electric drives," *IEEE Trans. Ind. Applicat.*, vol. 25, no. 6, pp. 1126–1131, Nov./Dec. 1989.

[19] W. Leonhard, *Control of Electrical Drives*, 2nd ed. Berlin, Germany: Springer, 1996.

[20] V.-M. Leppänen and J. Luomi, "Effect of equation of motion on low-frequency impedance of induction motors – an approach for rotor flux angle estimation," in *Proc. EPE-PEMC'02*, Cavtat and Dubrovnik, Croatia, Sept. 2002, CD-ROM.

[21] F. Briz, M. W. Degner, and R. D. Lorenz, "Analysis and design of current regulators using complex vectors," *IEEE Trans. Ind. Applicat.*, vol. 36, no. 3, pp. 817–825, May/June 2000.

[22] M. Hinkkanen and J. Luomi, "Parameter sensitivity of full-order flux observers for induction motors," *IEEE Trans. Ind. Applicat.*, vol. 39, no. 4, pp. 1127–1135, July/Aug. 2003.

[23] J. K. Pedersen, F. Blaabjerg, J. W. Jensen, and P. Thogersen, "An ideal PWM-VSI inverter with feedforward and feedback compensation," in *Proc. EPE'93*, vol. 4, Brighton, U.K., Sept. 1993, pp. 312–318.

[24] H. Kubota, I. Sato, Y. Tamura, K. Matsuse, H. Ohta, and Y. Hori, "Regenerating-mode low-speed operation of sensorless induction motor drive with adaptive observer," *IEEE Trans. Ind. Applicat.*, vol. 38, no. 4, pp. 1081–1086, 2002.

[25] T. Ohtani, N. Takada, and K. Tanaka, "Vector control of induction motor without shaft encoder," *IEEE Trans. Ind. Applicat.*, vol. 28, no. 1, pp. 157–164, Jan./Feb. 1992.

[26] H. Kubota, K. Matsuse, and T. Nakano, "DSP-based speed adaptive flux observer of induction motor," *IEEE Trans. Ind. Applicat.*, vol. 29, no. 2, pp. 344–348, Mar./Apr. 1993.

Marko Hinkkanen was born in Rautjärvi, Finland, in 1975. He received the M.Sc. degree in electrical engineering in 2000 from Helsinki University of Technology, Espoo, Finland, where he is currently working toward the D.Sc. degree.

Since 2000, he has been with the Power Electronics Laboratory, Helsinki University of Technology, as a research scientist. His main research interest is the control of electrical drives.

Veli-Matti Leppänen was born in Helsinki, Finland, in 1960. He received the M.Sc. (Eng.) and D.Sc. (Tech.) degrees from Helsinki University of Technology, Espoo, Finland, in 1985 and 2003, respectively. In 1985, he joined Strömberg Oy, which later became part of the ABB Group. He worked in ac drive product and technology development until 1999, when he joined the Power Electronics Laboratory in the Department of Electrical and Communications Engineering, Helsinki University of Technology. Currently, he is with ABB Oy in Helsinki. His research interests are in power electronics and sensorless control of induction motor drives.

Jorma Luomi (M'92) was born in Helsinki, Finland, in 1954. He received his M.Sc. (Eng.) and D.Sc. (Tech.) degrees from Helsinki University of Technology in 1977 and 1984, respectively.

In 1980 he joined Helsinki University of Technology, and from 1991 to 1998 he was a Professor at Chalmers University of Technology. As of 1998 he holds the position of Professor at the Department of Electrical and Communications Engineering at Helsinki University of Technology. His research interests are in the areas of electric drives, electric machines and numerical analysis of electromagnetic fields.